

## ARTICLE

<https://doi.org/10.1038/s42005-019-0168-y>

OPEN

# Gamma-ray glow preceding downward terrestrial gamma-ray flash

Yuuki Wada <sup>1,2,3</sup>, Teruaki Enoto <sup>2,4</sup>, Yoshitaka Nakamura<sup>5</sup>, Yoshihiro Furuta<sup>6</sup>, Takayuki Yuasa <sup>7</sup>, Kazuhiro Nakazawa <sup>8</sup>, Takeshi Morimoto <sup>9</sup>, Mitsuteru Sato<sup>10</sup>, Takahiro Matsumoto<sup>1</sup>, Daisuke Yonetoku<sup>11</sup>, Tatsuya Sawano<sup>11</sup>, Hideo Sakai<sup>12</sup>, Masashi Kamogawa<sup>13</sup>, Tomoo Ushio<sup>14</sup>, Kazuo Makishima<sup>1,2,15</sup> & Harufumi Tsuchiya<sup>16</sup>

Two types of high-energy events have been detected from thunderstorms. One is “terrestrial gamma-ray flashes” (TGFs), sub-millisecond emissions coinciding with lightning discharges. The other is minute-lasting “gamma-ray glows”. Although both phenomena are thought to originate from relativistic runaway electron avalanches in strong electric fields, the connection between them is not well understood. Here we report unequivocal simultaneous detection of a gamma-ray glow termination and a downward TGF, observed from the ground. During a winter thunderstorm in Japan on 9 January 2018, our detectors caught a gamma-ray glow, which moved for ~100 s with ambient wind, and then abruptly ceased with a lightning discharge. Simultaneously, the detectors observed photonuclear reactions triggered by a downward TGF, whose radio pulse was located within ~1 km from where the glow ceased. It is suggested that the highly-electrified region producing the glow was related to the initiation of the downward TGF.

<sup>1</sup>Department of Physics, Graduate School of Science, The University of Tokyo, 7-3-1, Hongo, Bunkyo-ku, Tokyo 113-8654, Japan. <sup>2</sup>High Energy Astrophysics Laboratory, RIKEN Nishina Center, 2-1, Hirosawa, Wako, Saitama 351-0198, Japan. <sup>3</sup>Laboratoire AstroParticule et Cosmologie, Université Paris Diderot, CNRS/IN2P3, CEA/DRF/IRFU, Observatoire de Paris, 10, rue Alice Domon et Léonie Duquet, 75013 Paris, France. <sup>4</sup>The Hakubi Center for Advanced Research and Department of Astronomy, Kyoto University, Kitashirakawa Oiwake-cho, Sakyo-ku, Kyoto 606-8302, Japan. <sup>5</sup>Department of Electrical Engineering, Kobe City College of Technology, 8-3, Gakuen-Higashimachi, Nishi-ku, Kobe, Hyogo 651-2194, Japan. <sup>6</sup>Collaborative Laboratories for Advanced Decommissioning Science, Japan Atomic Energy Agency, 2-4 Shirakata, Tokai-mura, Naka-gun, Ibaraki 319-1195, Japan. <sup>7</sup>Block 4B, Boon Tiong Road, Singapore 165004, Singapore. <sup>8</sup>Kobayashi-Maskawa Institute for the Origin of Particles and the Universe, Nagoya University, Furo-cho, Chikusa-ku, Nagoya, Aichi 464-8601, Japan. <sup>9</sup>Faculty of Science and Engineering, Kindai University, 3-4-1 Kowakae, Higashiosaka, Osaka 577-8502, Japan. <sup>10</sup>Graduate School of Science, Hokkaido University, Kita 8, Nishi 5, Kita-ku, Sapporo, Hokkaido 060-0808, Japan. <sup>11</sup>School of Mathematics and Physics, Kanazawa University, Kakuma, Kanazawa, Ishikawa 920-1192, Japan. <sup>12</sup>University of Toyama, 3190 Gofuku, Toyama, Toyama 930-0887, Japan. <sup>13</sup>Global Center for Asian and Regional Research, University of Shizuoka, 3-6-1, Takajo, Aoi-ku, Shizuoka, Shizuoka 420-0839, Japan. <sup>14</sup>Faculty of Systems Design, Tokyo Metropolitan University, 6-6 Asahigaoka, Hino, Tokyo 191-0065, Japan. <sup>15</sup>Kavli Institute for the Physics and Mathematics of the Universe, The University of Tokyo, 5-1-5 Kashiwa-no-ha, Kashiwa, Chiba 277-8683, Japan. <sup>16</sup>Nuclear Science and Engineering Center, Japan Atomic Energy Agency, 2-4 Shirakata, Tokai-mura, Naka-gun, Ibaraki 319-1195, Japan. Correspondence and requests for materials should be addressed to Y.W. (email: [wada@juno.phys.s.u-tokyo.ac.jp](mailto:wada@juno.phys.s.u-tokyo.ac.jp))

Since McCarthy and Parks<sup>1</sup> found radiation-dose enhancements inside thunderclouds with an airborne detector in 1980s, high-energy phenomena associated with thunderstorms have been detected inside the Earth's atmosphere and from space. Terrestrial gamma-ray flashes (TGFs) are burst-like emission with their photon energy extending up to 20 MeV that last for several hundred microseconds, coincident with lightning discharges. They were first detected from space by Compton Gamma-Ray Observatory<sup>2</sup>, and since then have been reported by many other satellites<sup>3–8</sup>. Similar phenomena but going downward have been found in recent years at ground level<sup>9–17</sup>. They, now called “downward TGFs”, share several features with TGFs observed from space, such as coincidence with lightning, sub-millisecond durations, and energy spectra extending to >10 MeV. Downward TGFs that contains enough photons above 10 MeV have been experimentally shown to trigger atmospheric photonuclear reactions, namely producing neutrons and positron-emitting radioactive nuclei<sup>13,14</sup>. These photoneutrons can be observed as a short-duration gamma-ray burst lasting for several hundreds of milliseconds, as they are absorbed by atmospheric nuclei via neutron-capture processes<sup>14,18</sup>.

Gamma-ray glows, also referred to as long bursts<sup>19</sup> or thunderstorm ground enhancements<sup>20</sup>, are energetic radiation from thunderclouds with energies up to tens of MeVs, lasting for a few seconds to several minutes. They have been observed by airborne detectors<sup>1,21–23</sup>, at mountain-top<sup>20,24–29</sup> and sea-level observation sites<sup>19,30–33</sup>. Gamma-ray glows usually coincide with passage of thunderclouds, and sometimes cease at the moment when lightning discharges take place<sup>1,21–23,34–38</sup>.

Although TGFs and gamma-ray glows are distinguished clearly by duration, brightness, and timing with regard to lightning discharges, both of them are thought to originate from a common fundamental mechanism, called relativistic runaway electron avalanches (RREAs<sup>39,40</sup>). According to Wilson's hypothesis<sup>41</sup>, seed electrons (provided by, e.g., cosmic rays) can be accelerated up to an energy of tens of MeVs in strong electric fields, producing secondary electrons. The number of multiplied and accelerated electrons exponentially increases, and the accelerated electrons finally emit bremsstrahlung gamma rays as they interact with ambient atmospheric nuclei. Dwyer<sup>42</sup> proposed additional electron-seeding processes by positrons and backscattered gamma rays into the RREA mechanism, called “relativistic feedback model”. This model can achieve a higher multiplication factor than that of a RREA alone, and thus are thought to explain extraordinarily high brightness of TGFs.

Despite an increasing number of respective observation samples of TGFs and gamma-ray glows, connections between them remain poorly understood. This is primarily because there has been no report of simultaneous detection of both, except for a very recent short report on a marginal detection<sup>17</sup>. In this paper, we report the first unequivocal simultaneous detection of them at sea level and discuss its implications.

## Results

**Observation of high-energy phenomena in winter thunderstorms.** The Gamma-ray Observation of Winter Thunderclouds (GROWTH) collaboration<sup>31,32,35,43</sup> has been engaged with a multi-point observation campaign of atmospheric high-energy phenomena in coastal areas of Japan Sea<sup>14,44</sup>. Winter thunderstorms in Japan are ideal targets to observe this type of phenomena due to their unique characteristics; most notably typical altitude of clouds is significantly lower than ordinary<sup>38,45,46</sup>, which makes sea-level observations of gamma-ray glows viable.

We have developed portable radiation detectors dedicated to the multi-point observation. They have a 25 cm × 8 cm × 2.5 cm

Bi<sub>4</sub>Ge<sub>3</sub>O<sub>12</sub> (BGO) scintillation crystal coupled with two photomultiplier tubes (PMTs; HAMAMATSU R1924A). Outputs from the PMTs are amplified, and then read out by a 50 MHz digitiser onboard a data acquisition system. The data acquisition system stores 20-μs waveforms of the amplified analogue outputs once a pulse is detected, and extracts the maximum and minimum value as well as the timing of the pulse (see also Detector calibration). The maximum value corresponds to the energies of the pulse, and the minimum the analogue baseline voltage. The data acquisition system also records counts of discarded photon events due to buffer overflow, which are used for dead-time correction. Three detectors were deployed at three observation sites in Kanazawa City, the capital of Ishikawa Prefecture, by the Japan Sea coast (Fig. 1) and have been operated since October 2016.

Lightning discharges were monitored by a broadband low-frequency (LF: 0.8–500 kHz) lightning mapping network (hereafter LF network), for which detectors are installed along Toyama Bay and in Noto peninsula. Another receiver in the extreme-low-frequency band (ELF: 1–100 Hz) is installed at Kuju, as summarised in the section Radio observations. We also utilise lightning location data of Japanese Lightning Detection Network (JLDN) operated by Franklin Japan Co., Ltd.

**Detection of gamma-ray glow and downward TGF.** On 9 January 2018, two of our detectors shown in Fig. 1 recorded gamma-ray glows. Figure 2a, b shows long-term count-rate histories of detectors A and B, respectively. At around 17:54 in coordinated universal time (UTC), detector A at Kanazawa Izumigaoka High School (36.538°N, 136.649°E) recorded a radiation increase for ~60 s. Then, ~30 s later, detector B at Kanazawa University High School (36.539°N, 136.664°E, 1.3 km east from detector A) also recorded a gamma-ray glow. No radiation enhancements were observed by detector C at Kanazawa University Kakuma Campus (36.546°N, 136.709°E; 4 km from detector B) in the period. The glow then suddenly terminated, coincident with a lightning discharge, while it was still being observed by detector B.

An snapshot image of the X-band radar network at 17:55 shows a heavy precipitation area, corresponding to a thundercloud, located between detectors A and B (Fig. 1a). The radar data suggest that the thundercloud passed over the two detectors towards east-northeast with a speed of  $19.3 \pm 1.4 \text{ m s}^{-1}$  (see Wind estimation with X-band radar). Since the temporal separation between the glow detection by the two detectors is consistent with the time for the thundercloud to travel the distance between the two detectors, we consider that the gamma-ray glows recorded by the two detectors are from the same cloud and hence of the same origin.

At the same time as the glow termination and the lightning discharge, both detectors A and B recorded a short-duration radiation burst lasting for ~200 ms simultaneously. The count-rate profiles of the 200-ms-lasting short burst shown in Fig. 2c, d exhibit a steep rise and decay with time constants of  $52.0 \pm 4.9$  and  $59.2 \pm 1.7$  ms for detectors A and B, respectively. Combining the timing analysis with spectral analysis (see Gamma-ray emission originating from neutrons), the short burst is found to originate from neutron captures by atmospheric nitrogen nuclei, which Rutjes et al.<sup>18</sup> predicted as “TGF afterglow”, and Enoto et al.<sup>14</sup> observationally demonstrated. In addition, detector B recorded a faint annihilation emission at 511 keV for 10 s after the short burst (see Positron production by beta-plus decay). These features imply that atmospheric photonuclear reactions such as  $^{14}\text{N} + \gamma \rightarrow ^{13}\text{N} + n$  and  $^{16}\text{O} + \gamma \rightarrow ^{15}\text{O} + n$  took place coincident with the lightning discharge, as discussed in Bowers et al.<sup>13</sup> and Enoto et al.<sup>14</sup>.

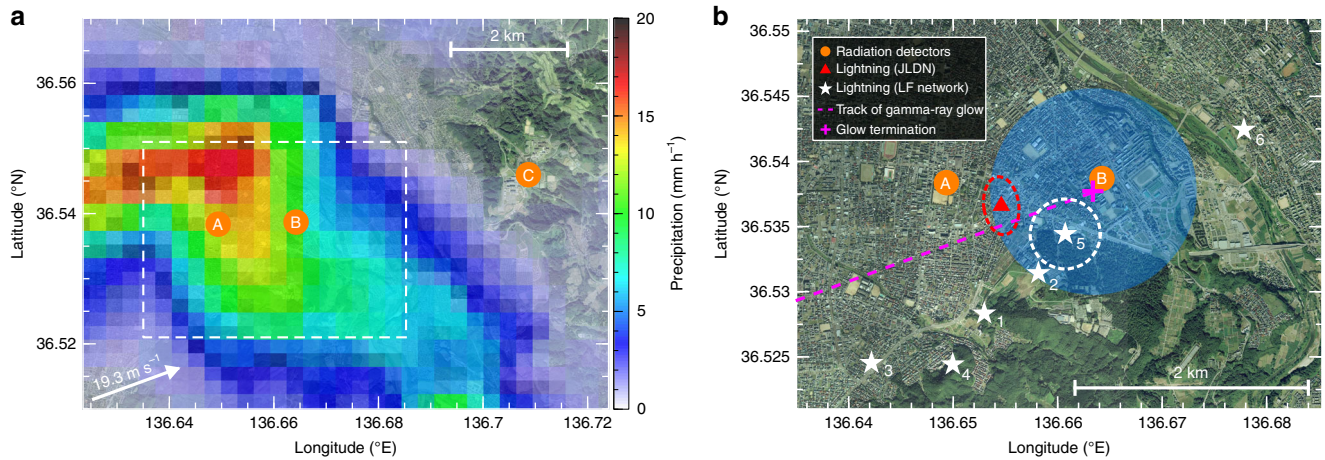


**Fig. 1** Maps of observation sites in Kanazawa. **a** A precipitation map at 17:55 on 9 January 2018 in coordinated universal time, obtained by the extended radar information network. Orange circles show radiation monitors, the white arrow the wind speed and its direction, and the dashed-line rectangle the region of panel **b**. **b** A panoramic photograph around detectors A and B marked by filled orange circles. The lightning locations determined by Japanese Lightning Detection Network and our low-frequency network are marked by red triangles and white stars, respectively. The numbers beside the white stars correspond to the order of the low-frequency pulses. A typical locating error circle ( $\sim 300$  m in radius) is overlaid for the fifth pulse. The magenta dashed line shows a track of the centre of the gamma-ray glow, which ceased at the magenta cross marker. The shaded blue circle shows the region where 30-s-binned count rates in the 3.0–20.0 MeV band reached twice or more higher than the background rates when the glow disappeared, estimated with the simulation (see Simulation of gamma-ray glow). This corresponds to a detection significance of  $8.1\sigma$  or higher. The radius of the region is 0.88 km. The background photographs are provided by the Geospatial Information Authority of Japan

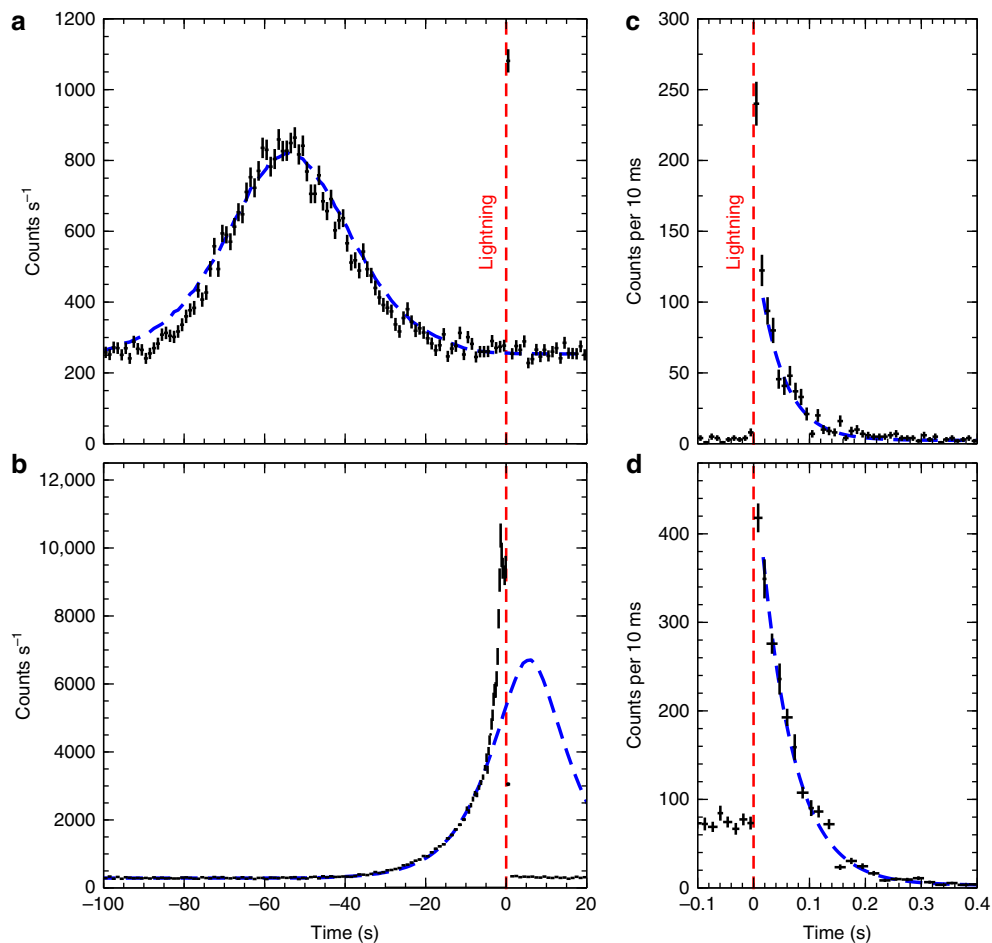


**Fig. 2** Count-rate histories of gamma-ray glow and short-duration burst. **a, b** One-sec-binned histories of detectors A (**a**) and B (**b**) at around the events with  $\pm 1\sigma$  statistical errors for an energy range of 0.4–20.0 MeV. The origin of the X axis is 17:54:50.308892 in coordinated universal time. Blue lines show the best-prediction profile from Monte Carlo simulations. Red dashed lines show the timing of the lightning discharge. **c, d** Histories with finer bins for the same energy band. Blue lines show the best-fitting model of an exponential function with time constants of  $52.0 \pm 4.9$  and  $59.2 \pm 1.7$  ms for detectors A and B, respectively

Figure 3a, b shows the maximum and minimum waveform values of photon events during the short burst recorded by detectors A and B, respectively. At the very beginning of the short burst, both detectors A and B recorded saturated pulses (the maximum values exceeding  $>4$  V), and then significant negative values of the baseline (the minimum values) called “undershoot” for  $\sim 10$  ms. Although detector B failed to acquire the main part of the undershoot due to buffer overflow in the data acquisition system, it recorded the saturated pulses and the last part of the undershoot. As demonstrated in Methods: Initial flash of Enoto et al.<sup>14</sup>, this feature manifests the existence of an extremely large energy deposit (much more than hundreds of

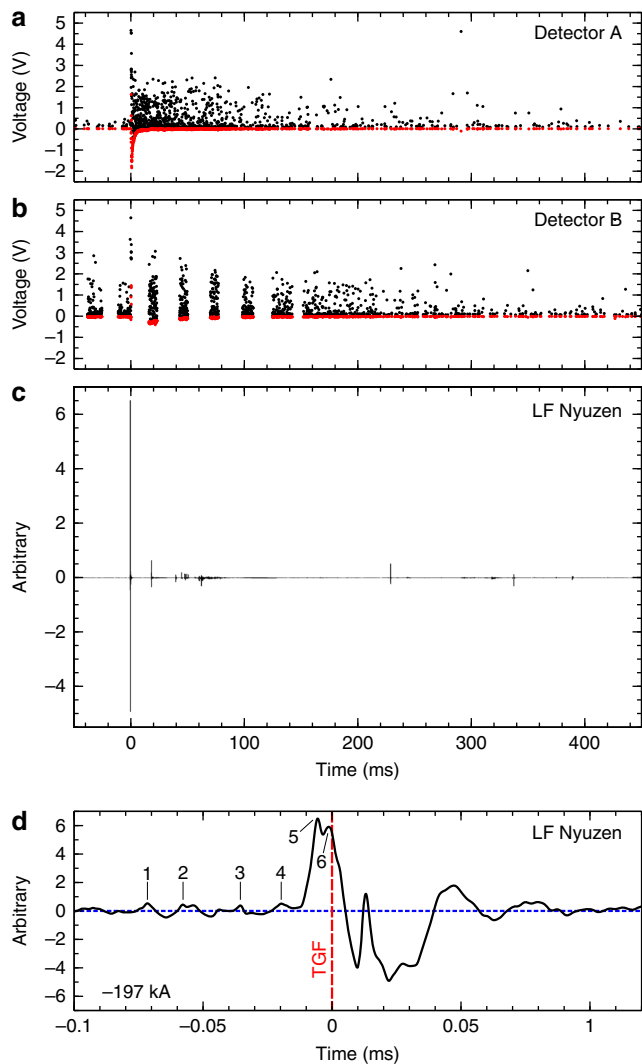


**Fig. 3** Signature of downward terrestrial gamma-ray flash and associated lightning pulse. **a, b** Time histories of the (black) maximum and (red) minimum values of high-energy radiation waveforms recorded by detector A (**a**) and detector B (**b**). The minimum values normally present the baseline of the analogue waveforms. An energy of 10 MeV corresponds to 2.3 V in the normal (non-disturbed) operation condition. The time origin is at the TGF detection. **c** The low-frequency waveform (LF) of the lightning discharge recorded by the Nyuzen station (36.954°N, 137.498°N). The propagation time between the locations of the source of the large-amplitude pulse and the observation station is corrected. **d** LF waveform of the large-amplitude pulse associated with the downward TGF for a sub-millisecond period. Blue dashed line shows the waveform baseline. Number-assigned pulses are used for the location analysis

MeVs) in the scintillation crystal within a few milliseconds, which is a clear sign of a downward TGF. In the following analysis we employ an elapsed time  $t$  from the onset of the downward TGF at 17:54:50.308892 UTC, recorded by detector B.

The LF network recorded a consecutive series of waveforms of the lightning discharge lasting for  $\sim 400$  ms (Fig. 3c). The downward TGF coincided with a large-amplitude pulse at the initial phase of the lightning discharge within 10  $\mu$ s (Fig. 3d). We detected four or so precursory pulses shortly before the large-amplitude pulse. No pulses had been detected before the precursory pulses by the LF network. The ELF measurement also confirmed that the associated ELF pulse was coming from the LF source. In addition, JLDN also reported a negative intracloud/intercloud (IC) discharge of  $-197$  kA at  $t = -13$   $\mu$ s, which is temporally associated with the large-amplitude pulse.

Figure 1b shows the source positions of the large-amplitude and precursory pulses determined by the LF network. At the beginning, the small precursory pulses took place in a southwest region less than 3 km away from detector B. Then, the main large-amplitude pulse (the fifth one in Figs. 1b and 3c) occurred 0.6 km southwest of detector B at  $t = -5.5$   $\mu$ s. JLDN also located the large-amplitude pulse within 0.9 km from detector B. These temporal and spatial correlations lead us to conclude that the large-amplitude LF pulse is associated with the downward TGF.

**Production mechanism of gamma-ray glow.** The multi-point observation enables us to investigate characteristics of the gamma-ray glow preceding the lightning initiation and the downward TGF. First, we perform spectral analysis. Figure 4 shows the background-subtracted gamma-ray energy spectra, extracted from  $-69$  s  $< t < -39$  s and  $-30$  s  $< t < -10$  s for detectors A and B, respectively. The detector response function is calculated with the GEANT4 Monte Carlo simulation framework<sup>47</sup>, and is convolved with a model spectrum in spectral fitting using the XSPEC package<sup>48</sup>. The observed spectra, of which instrumental responses are corrected, are found to be well explained by an empirical power-law function with an exponential cutoff,  $\varepsilon^{-\Gamma} \exp[-\varepsilon/\varepsilon_{\text{cut}}^\alpha]$ , where  $\varepsilon$ ,  $\Gamma$ ,  $\varepsilon_{\text{cut}}$ , and  $\alpha$  are the photon energy (MeV), power-law photon index, cutoff energy (MeV), and cutoff index, respectively. The best-fitting parameters are  $\Gamma = 0.90^{+0.06}_{-0.08}$  and  $1.02^{+0.04}_{-0.05}$ ,  $\varepsilon_{\text{cut}} = 6.4^{+1.0}_{-1.1}$  and  $8.5^{+0.8}_{-0.9}$  MeV,

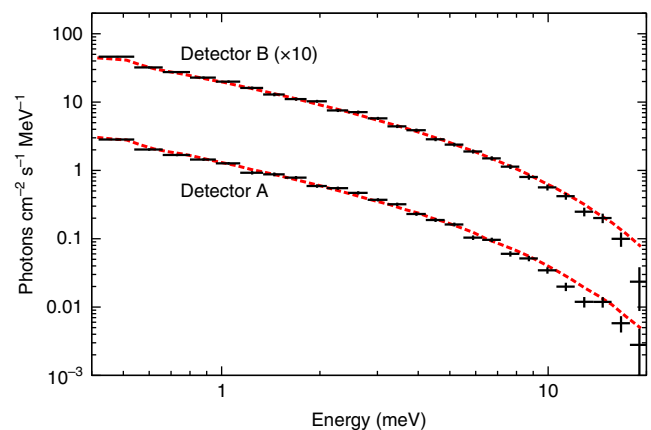


**Fig. 4** Energy spectra of gamma-ray glow. Background-subtracted and deadtime-corrected energy spectra of the gamma-ray glow for the time region from  $-69$  s  $< t < -39$  s and  $-30$  s  $< t < -10$  s for detectors A (lower) and B (upper), respectively, where  $t$  is defined in text and is used in Fig. 2. The error of each data point is at  $1\sigma$  confidence level. The spectrum of detector B is shifted upwards by a factor of 10 for visibility. The best-fitting model of the Monte Carlo simulation is overlaid with red dashed lines

$\alpha = 1.21_{-0.14}^{+0.15}$  and  $1.43_{-0.14}^{+0.15}$ , and the 0.4–20.0 MeV incident gamma-ray flux of  $1.5_{-0.5}^{+0.7} \times 10^{-5}$  and  $2.4_{-0.6}^{+0.7} \times 10^{-5}$  ergs cm<sup>-2</sup> s<sup>-1</sup> on average over  $-69 \text{ s} < t < -39 \text{ s}$  and  $-30 \text{ s} < t < -10 \text{ s}$  integration periods for detectors A and B, respectively. Here and after, all the errors are statistical at  $1\sigma$  confidence level, unless otherwise mentioned.

We then perform another set of Monte Carlo simulations, using GEANT4, and compare the obtained energy spectra and count-rate histories with the simulated ones to investigate atmospheric interactions and propagation of electrons and gamma rays (see Simulation of gamma-ray glow). We find a model of spatial and energy spectral distribution for avalanche electrons in the RREA region which can reproduce both the obtained gamma-ray spectra and count-rate histories, and summarise the results in Figs. 1 and 4. The best-fit value of the RREA terminus altitude  $h_{\text{base}}$  is 400 m, which means the electron avalanche took place in the lower part of the winter thundercloud, and the offsets from the centre of the RREA region are 540 and 80 m for detectors A and B, respectively. The electron flux distribution is consistent with being proportional to a function of a distance from the RREA centre  $r$ ,  $\exp(-r/150 \text{ m})$ , providing the circularly symmetric distribution. Figure 1b shows the centre position of the RREA region at the moment of the termination. Normalising the simulation result, we estimate the total production rate of 1–50 MeV avalanche electrons to be  $3.66 \times 10^{12}$  electrons s<sup>-1</sup>. The electron flux  $F(r, \epsilon)$  at the terminus of RREA is also estimated to be a function of  $r$  and  $\epsilon$

$$F(r, \epsilon) = 4.1 \times 10^2 \exp\left(-\frac{r}{150 \text{ m}}\right) \exp\left(-\frac{\epsilon}{7.3 \text{ MeV}}\right) \text{ electrons cm}^{-2} \text{ s}^{-1} \text{ MeV}^{-1}. \quad (1)$$

This model reproduces the observed count-rate histories and spectra, except the increase in the count rate of detector B during  $-5 \text{ s} < t < 0 \text{ s}$ . This period is discussed in the section Abrupt increase in count rates of gamma-ray glow before downward TGF.

Let us consider the electron multiplication factor  $M = F_{\text{RREA}}/F_{\text{seed}}$ , where  $F_{\text{RREA}}$  and  $F_{\text{seed}}$  are the average electron flux at the RREA terminus and seed electron flux, respectively. Integrating Eq. (1) yields the 0.3–50 MeV average flux within  $r = 150 \text{ m}$  of  $F_{\text{RREA}} = 7.5 \times 10^2$  electrons cm<sup>-2</sup> s<sup>-1</sup>. Assuming that the seed electrons are mainly produced by cosmic rays, the 0.3–50 MeV seed electron flux is a function of a vertical acceleration length  $L$  and  $h_{\text{base}}$  given by

$$F_{\text{seed}}(L) = 2.56 \times 10^{-3} \exp[(L + h_{\text{base}})/1890 \text{ m}] \text{ electrons cm}^{-2} \text{ s}^{-1} \quad (2)$$

(see Seed electrons). The multiplication factor  $M$  is thus a function of  $L$ , with the fixed  $h_{\text{base}}$  (400 m).

In the RREA region, electron flux is known to increase<sup>39</sup> exponentially as a function of  $L$ ,  $F_{\text{RREA}} = F_{\text{seed}} \exp(L/\lambda)$ , assuming that change of the vertical atmospheric pressure is negligible for the RREA processes at the low altitude. The avalanche length  $\lambda$  is empirically determined (see ref. 49 and references therein) to be  $\lambda = 7.3 \text{ MeV}/(eE - 0.276 \text{ MeV m}^{-1})$ , where  $eE$  is a product of the elementary charge and strength of the electric field. The value of  $\lambda$  is then calculated to be 304, 99, and 59 m for  $E = 0.3, 0.35,$  and  $0.4 \text{ MV m}^{-1}$ , respectively. We note that the set of the trial values of  $E$  up to  $0.4 \text{ MV m}^{-1}$  we have assumed is suggested to be plausible inside thunderclouds<sup>39</sup>. Therefore, combining  $M(L) = F_{\text{RREA}}/F_{\text{seed}}(L) = \exp(L/\lambda)$ ,  $L$  and  $M$  are derived to be  $L = 3240, 1160,$  and  $710 \text{ m}$ ,  $M = 4.3 \times 10^4, 1.3 \times 10^5,$  and  $1.6 \times 10^5$  for  $E = 0.3, 0.35,$  and  $0.4 \text{ MV m}^{-1}$ , respectively.

As Dwyer<sup>50</sup> pointed out, the multiplication factor would not exceed  $\sim 10^5$  in the RREA-only case because thunderclouds

cannot maintain an acceleration length required for it. Given that  $L$  can reach twice as high as the typical diameter of the RREA region<sup>50</sup>,  $L < 600 \text{ m}$  is required in this case, where the typical radius  $r = 150 \text{ m}$  is employed. The  $0.3 \text{ MV m}^{-1}$  case is not plausible because the required acceleration length  $L = 3240 \text{ m}$  cannot be maintained inside the thundercloud. In the other cases, it is necessary to take into account the relativistic feedback processes to explain the estimated avalanche multiplication factor. The relativistic feedback processes are parameterised with a feedback factor  $\gamma$ , the fraction of the seed electrons provided by the steady-state relativistic feedback processes<sup>50</sup>. The flux of runaway electrons is then modified as  $F_{\text{RREA}} = F_{\text{seed}}(L) \exp(L/\lambda)/(1 - \gamma)$ . Figure 5 shows this relation between  $L$  and  $\gamma$  to explain the observed flux at the RREA terminus. To satisfy the condition  $L < 600 \text{ m}$ ,  $\gamma$  should be larger than 0.998 and 0.846 for 0.35 and  $0.4 \text{ MV m}^{-1}$ , respectively. This suggests that the number of feedback-origin seed electrons is higher than that of cosmic-ray seed electrons by a factor of  $>5.5$  for our event.

### Abrupt increase in count rates of gamma-ray glow before TGF.

The count-rate history of detector B exhibited an additional increase during  $-5 \text{ s} < t < 0 \text{ s}$  (Fig. 6a). Figure 6b shows the ratio of the simulated model to the observed history. Although the observed history is well reproduced by the simulation up to  $t = -5 \text{ s}$ , the observed count rate is twice as high as the simulation in  $-5 \text{ s} < t < 0 \text{ s}$ . Figure 6c shows the three energy spectra extracted from the time regions of  $-10 \text{ s} < t < -5 \text{ s}$ ,  $-5 \text{ s} < t < -2 \text{ s}$ , and  $-2 \text{ s} < t < 0 \text{ s}$ . All the spectra show a power-law function with an exponential cutoff, indicating that bremsstrahlung is still the main process of gamma-ray production. Since our simulations fail to reproduce this increase in count-rate, we speculate that the increase was caused by a fluctuation of the intrinsic electron fluxes, rather than by the movement of the RREA region with the ambient wind flow.

Based on the working hypothesis of the speculated increase of the accelerated electron flux, at least one of the following is required to have taken place: (1) stronger electric fields of the RREA region, (2) longer acceleration length, and/or (3) increase in the feedback factor  $\gamma$ . However, since lightning did not occur during this period ( $-5 \text{ s} < t < 0 \text{ s}$ ), atmospheric mechanism could not drastically change the meteorological conditions, such as electric fields and acceleration length, within 5 s. We thus

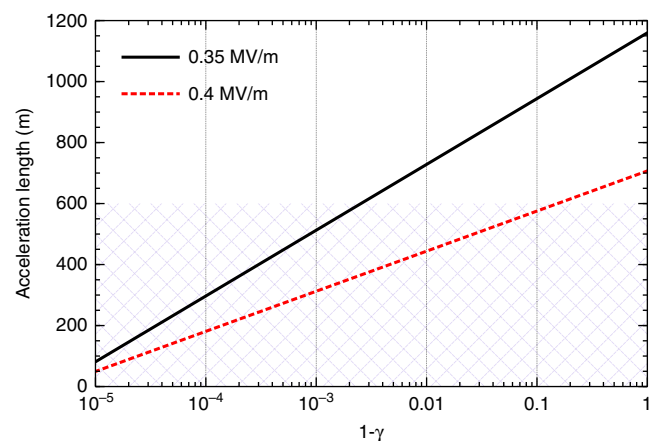


**Fig. 5** Properties of relativistic runaway electron avalanche with relativistic feedback. The acceleration length as a function of the feedback factor  $\gamma$ . Black solid and red dashed lines indicate the cases with the electric field strengths of  $E = 0.35$  and  $0.4 \text{ MV m}^{-1}$ , respectively. The blue-meshed region shows the plausible acceleration length in the case considered in this paper

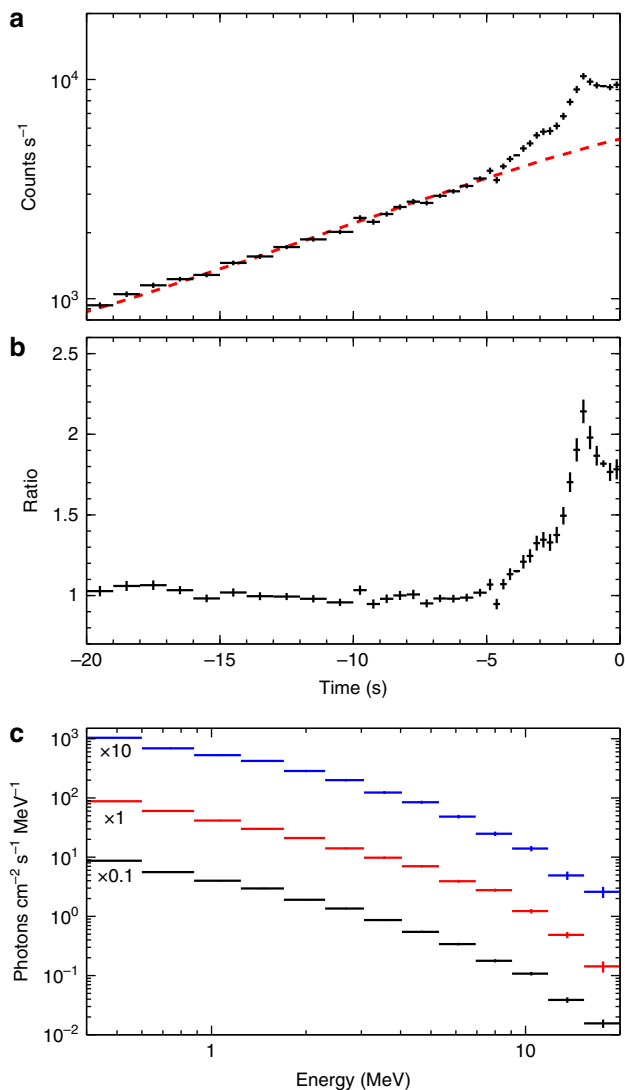


**Fig. 6** Increase in count rates of detector B. **a** Comparison between the count-rate history of detector B and the exponential model (red dashed line). Background was subtracted. **b** Ratio of the Gaussian model to the observed count-rate history. **c** Background-subtracted spectra of detector B extracted from (black)  $-10\text{ s} < t < -5\text{ s}$ , (red)  $-5\text{ s} < t < -2\text{ s}$ , and (blue)  $-2\text{ s} < t < 0\text{ s}$ . The error of each data point is at  $1\sigma$  confidence level. The spectra in  $-10\text{ s} < t < -5\text{ s}$  and  $-2\text{ s} < t < 0\text{ s}$  are shifted by a factor of 0.1 and 10, respectively, to avoid overlapping. Dead-time and detector responses are corrected

conjecture that temporal variations of the relativistic feedback processes played an important role for the electron flux increase, then the abrupt rise of gamma rays in the 5-s period before the lightning discharge. Assuming the electric field of  $0.4\text{ MV m}^{-1}$ , the doubled rate of avalanche electrons can be explained by increasing  $\gamma$  from 0.846 to 0.923.

The RREA and relativistic feedback processes remained stable until  $t = -5\text{ s}$ ; this state corresponds to the “steady state” of relativistic feedback as defined by Dwyer<sup>50</sup>, namely  $\gamma < 1$ . In general, when  $\gamma$  exceeds 1, an electron flux would spontaneously increase, and an RREA region should collapse. The timescale of the flux increase depends on the types of the relativistic feedback processes. The feedback process by positrons can discharge RREA regions within microseconds<sup>50</sup>. This timescale is close to that of TGFs, and is much shorter than that of the observed abrupt increase (i.e. 5 s). Alternatively, the feedback by backscattered

X-rays may trigger a second-order discharge in RREA regions<sup>50</sup>. At present, even though the 5-s abrupt flux rise seems to be of great importance, its origin is yet to be understood.

## Discussion

To conclude the relation between the gamma-ray glow and the downward TGF, verifying their temporal and positional coincidence will give a strong clue. Our observation cannot clarify whether the glow termination or the downward TGF took place first because these phenomena seemed to be slightly overlapped. On the other hand, the positional coincidence of the gamma-ray glow and the downward TGF in the present case is precisely determined owing to the multiple gamma-ray detectors and the LF network. The discussion in the section Production mechanism of gamma-ray glow suggests that the gamma-ray glow ceased when the source cloud was moving 130 m southwest of detector B (Fig. 1b). Also, the TGF-associated LF pulse was located within 0.5 km from detector B. Therefore, it is clear that the two phenomena are physically related to one another.

Our interpretation of the observed gamma-ray glow suggests that the electron acceleration site should have electric fields of  $0.35\text{ MV m}^{-1}$  or higher in order to achieve the high electron multiplication factor of  $>10^5$  with a plausible acceleration length. In such highly electrified regions, TGFs are thought to initiate more easily than in other less-electrified regions as Smith et al.<sup>17</sup> suggested. From another point of view, we speculate that the avalanche electrons of the gamma-ray glow can behave as seed electrons of the downward TGF. At the point where the TGF-associated LF pulse was located (point 5 in Fig. 1b), the 0.3–50 MeV electron flux at 400 m altitude is estimated to be  $1.7 \times 10^2\text{ electrons cm}^{-2}\text{ s}^{-1}$ . By comparing this flux with that of the cosmic-ray-induced seed electrons (the canonical seed electron source), it is suggested that the highly-electrified region responsible for the gamma-ray glow can be the dominant source of seed electrons for the TGF which occurs in the close proximity of the gamma-ray glow. In addition, the abrupt count-rate increase monitored by detector B before the TGF (see section Abrupt increase in count rates of gamma-ray glow before downward TGF) suggests additional production of avalanche electrons for the gamma-ray glow, and might have predicted drastic changes in the electrified region such as the lightning discharge and the TGF.

In the present high-energy event, the discussion above suggests a possibility that the high electron current in the gamma-ray glow assisted the initiation of the downward TGF. However, it still remains observationally unclear how gamma-ray glows and TGFs are related with each other in general. Among an increasing sample of glow terminations, TGF-associated events are still quite rare, i.e. only Smith et al.<sup>17</sup> and the present event. For example, a termination event during a winter thunderstorm in 2017 (ref. 38) was associated with an intracloud/intercloud discharge but not related with any signals for TGF-like emissions. As another example, a TGF-like intensive emission associated with photonuclear reactions was reported<sup>14</sup>, where no gamma-ray glows were recorded before the event. In these cases, we lack sufficient evidences due to our present sparse observation sites on the ground to conclude that glow terminations are not always associated with TGFs. Our future gamma-ray monitoring network combined with radio-frequency lightning mapping systems will give a clue to reveal the relation between TGFs and gamma-ray glows.

In summary, we detected a gamma-ray glow, terminated with a downward TGF which triggered atmospheric photonuclear reactions. The gamma-ray glow was so bright that the relativistic feedback processes are required. Although we cannot determine whether the glow termination or the downward TGF occurred

first, the two high-energy phenomena in the atmosphere took place in an identical electrified region of a winter thundercloud, and hence are clearly related to each other in the present case.

## Methods

**Detector calibration.** Energy calibration of the detectors was performed to convert the maximum value of a pulse into photon energy. We measured the centre of environmental background lines of  $^{40}\text{K}$  (1.46 MeV) and  $^{208}\text{Tl}$  (2.61 MeV), and built a linear calibration function which is utilised to assign the energy of each photon. All the detectors record 0.4–20.0 MeV gamma rays. See also Instrumental calibration in Enoto et al.<sup>14</sup> for details.

Absolute timing is conditioned by pulse-per-second signals of the Global Positioning System (GPS). The timing-assignment logic employed from 2017 to 2018 winter provides absolute timing accuracy of each photon better than 1  $\mu\text{s}$ . However, detector A failed to receive the GPS signals during the experiment. Instead, we performed the calibration of detector A, using the internal clock time with  $\sim 1$  s accuracy, and then corrected the absolute timing so that the detection time of the downward TGF matches that with detector B.

**Wind estimation with X-band radar.** We utilised data of eXtended RADar Information Network (XRAIN). XRAIN is a polarimetric weather radar network in the X band and has a spatial resolution of 280 m (east–west)  $\times$  230 m (north–south) mesh. It records two-dimensional precipitation maps with a 1-min interval. XRAIN also obtains three-dimensional maps of radar echoes and particle types with a 5-min interval by the constant-altitude plan position indicator technique. However, the three-dimensional data are not utilised in the present paper because the XRAIN observations have a moderate spatial resolution of altitude ( $\geq 1$  km), which is insufficient to discuss charge structures in the thundercloud.

Wind velocity and direction are estimated by overlaying and shifting precipitation maps at different time. First, 11 maps from 17:50 to 18:00 were extracted in the range of 36.4°N–36.7°N, 136.4°E–136.8°E. We then took a pair of maps with a 5-min interval (six pairs in total), and calculated the sum of precipitation residual at each mesh, given by  $\sum_{i,j}(P_{ij}^1 - P_{ij}^2)^2$ , where  $P_{ij}^1$  and  $P_{ij}^2$  are precipitation at each mesh on each map, and  $i$  and  $j$  are mesh indexes. With trial shifting of one map with several steps of the spatial resolution for four directions, we searched for the position which takes the minimum residual sum. The distance and direction for which the cloud moved in 5 min can be estimated from the amount of the map shift at the point of the minimum residual sum. Consequently, the wind direction and velocity at the moment of the glow detection were determined to be west-northwestwards and  $19.3 \pm 0.9$  (systematic)  $\pm 1.1$  (statistic)  $\text{m s}^{-1}$ , respectively. Here, the quoted statistical error was calculated from the standard deviation ( $1\sigma$ ) of six pairs. The systematic error was determined by the mesh size and temporal interval of the map pair. The wind velocity with the overall error is then calculated to be  $19.3 \pm 1.4 \text{ m s}^{-1}$ , where the standard error propagation in quadrature between the systematic and statistical errors is assumed to hold. Since the statistic error is smaller than 10% and is comparable with the systematic error, it is reasonable to assume that the wind parameters did not change considerably during the glow observation.

**Gamma-ray emission originating from neutrons.** Photonuclear reactions such as  $^{14}\text{N} + \gamma \rightarrow ^{13}\text{N} + n$  and  $^{16}\text{O} + \gamma \rightarrow ^{15}\text{O} + n$  expel  $\sim 10$  MeV neutrons from atmospheric nitrogen and oxygen nuclei<sup>51–53</sup>. The photonucleons gradually lose their kinetic energy via elastic scatterings, and are eventually captured by atmospheric nuclei such as  $^{14}\text{N}$ . In the dominant reaction  $^{14}\text{N} + n \rightarrow ^{15}\text{N} + \gamma$ ,  $^{15}\text{N}$  nuclei in excited states emit various de-excitation gamma-ray lines up to 10.8 MeV. In addition, de-excitation gamma rays from other nuclei such as Si and Al should be also emitted when photonucleons were captured by ambient nuclei in soil, buildings, and components of the detectors. These de-excitation gamma rays originating from neutron captures are thought to compose the short burst<sup>14,18</sup>.

The timescale of the short burst is determined by neutron thermalisation<sup>13,14,18</sup>. A numerical calculation predicts the neutron-capturing rate of  $\exp(-t/\tau)$  for 5 ms  $< t < 120$  ms, where  $t$  is the elapsed time from the onset of the TGF and  $\tau \approx 56$  ms is the decay constant<sup>14</sup>. The count-rate histories of the observed burst have decay constants of  $52.0 \pm 4.9$  and  $59.2 \pm 1.7$  ms for detectors A and B, respectively. These results are consistent with the calculation.

Supplementary Fig. 1 shows the energy spectra of the burst with detectors A and B. Enoto et al.<sup>14</sup> simulated the de-excitation emission, considering atmospheric scattering of the gamma rays and moderate energy resolution of BGO crystals. The emission model from  $^{15}\text{N}$  and ambient nuclei, such as Al and Si, well reproduces the results of both detectors A and B. From the spectral and temporal analyses, we confirm that the observed short burst is caused by neutrons produced via atmospheric photonuclear reactions.

**Positron production by beta-plus decay.** After neutrons are expelled from  $^{14}\text{N}$  and  $^{16}\text{O}$ , unstable nuclei  $^{13}\text{N}$  and  $^{15}\text{O}$  start emitting positrons via  $\beta^+$  decay with half-lives of 10 and 2 min, respectively. Positrons immediately annihilate and emit 511 keV annihilation gamma rays. Supplementary Fig. 2a–d shows count-rate histories in the 0.4–0.65 and 0.65–30.0 MeV bands. Whereas detector A recorded

no enhancements after the short burst, detector B recorded an afterglow in the 0.4–0.65 MeV band for the period  $0 \text{ s} < t < 10 \text{ s}$ . The count rates decreased with a decay constant of  $6.0 \pm 2.1 \text{ s}$ . The background-subtracted photon count in the 0.4–0.65 MeV band for  $1 \text{ s} < t < 10 \text{ s}$  is  $(2.0 \pm 0.4) \times 10^2$  photons. The background-subtracted energy spectrum is shown in Supplementary Fig. 2e. The centre energy of the line emission is  $528 \pm 14 \text{ keV}$ , which is consistent with 511 keV of the annihilation line within error.

These results lead us to conclude that a positron-emitting region filled with  $^{13}\text{N}$  and  $^{15}\text{O}$  were produced in the atmosphere by the photonuclear reactions, and then passed over detector B flown by the ambient wind flow<sup>14</sup>. Considering that the count-rate history shows a monotonic decrease, the positron source might be generated somewhere above detector B or downwind.

**Radio observations.** The LF network has five stations (Supplementary Fig. 3a). Each station has a flat plate antenna sensitive to 0.8–500 kHz. Analogue outputs from the antenna are sampled by a 4 MHz digitiser, whose absolute timing is calibrated with the GPS signals. The LF network can locate radio pulses with the time-of-arrival technique. Supplementary Fig. 3b, c shows the entire LF waveforms of the observed lightning discharge.

The ELF receiver is installed in Kuju (33.059°N, 131.233°E) as a station of the Global ELF Observation Network operated by Hokkaido University. The station has two horizontal search coil magnetometers sensitive to 1–100 Hz magnetic-field perturbations in the east–west and north–south directions. The analogue output is sampled by a 400 Hz digitiser. The direction-of-arrival of the ELF pulses can be confirmed with the magnetic-detection-finder technique. Supplementary Fig. 3d shows the observed waveform in the ELF band.

The JLDN reported two other discharges besides the TGF-associated radio-frequency pulse: an IC of  $-14 \text{ kA}$  at  $t = 18.7 \text{ ms}$  and a CG of  $-13 \text{ kA}$  at  $t = 228.6 \text{ ms}$ . Supplementary Fig. 3b, c shows the corresponding LF pulses. Since these pulses occurred long after the observed TGF, we consider that they were not associated with the high-energy phenomena.

**Simulation of gamma-ray glow.** We performed Monte Carlo simulations of electron propagation in the atmosphere to reproduce the count-rate histories and energy spectra, using GEANT4 (ref. 47). We assume that electron avalanches towards the ground developed in thundercloud, and that the electron spectrum of the RREA at the end of the region has the shape of  $\exp(-\epsilon/7.3 \text{ MeV})$ <sup>49</sup>, where  $\epsilon$  is the electron energy. We also assume that the distribution of the electron flux in the avalanche region is circularly symmetric and has no intrinsic time fluctuation. These assumption should be reasonable, given that the count-rate history of detector A is symmetric about the peak, and that the wind velocity was approximately constant (see Wind estimation with X-band radar).

The energy spectra of bremsstrahlung gamma rays from the avalanche electrons approximately follow  $\epsilon^{-1}\exp(-\epsilon/7.3 \text{ MeV})$ <sup>54</sup>. The photon index  $\Gamma$  is determined from the source altitude  $h$  and offset from the source centre. Count-rate histories depend on the size of the RREA region, wind velocity, and  $h$ . The distribution of gamma rays is more diffuse at a higher source altitude due to atmospheric scattering, hence resulting in a longer and fainter gamma-ray glow.

First, we tested a disk-like region with a uniform electron flux, varying  $h$  and disk radius in our simulations. Supplementary Fig. 4a shows some examples of the simulation results at various altitudes. Comparing the simulation results with the observation,  $h = 1500 \text{ m}$  is required to reproduce the observed count-rate histories, whereas  $\Gamma$  of the energy spectra indicates  $h = 900 \text{ m}$ . Since any other conditions cannot satisfy both the spectra and count-rate histories, this uniform-disk model is thus rejected in this analysis.

Then, we considered two disk-like models in which the spatial distribution of the electron flux follows either of the two functions of a distance from the RREA centre  $l$ : a Gaussian model,  $\exp(-l^2/2\sigma^2)$  and an exponential model,  $\exp(-l/L)$ . The parameters  $\sigma$  and  $L$  are free parameters, which denote the spatial extent of the surface brightness of the emission.

We found that both models can reproduce the obtained count-rate histories and spectra; The estimated parameters are  $h = 600 \text{ m}$  and  $\sigma = 200 \text{ m}$  for the Gaussian model, and  $h = 400 \text{ m}$  and  $L = 150 \text{ m}$  for the exponential model. Comparing these two best models, we found that the exponential model explains the observation better, particularly for the count-rate histories of detector B (Supplementary Fig. 4b). Therefore, we employ the exponential model as a working hypothesis to interpret the observation.

**Seed electrons.** We assume that the seed electrons of the RREA processes are mainly produced by cosmic rays. To calculate the electron fluxes of secondary cosmic rays, we employed Excel-based Program for calculating Atmospheric Cosmic-ray Spectrum (EXPACS)<sup>55,56</sup>, which calculates the flux and spectrum of cosmic-ray particles as a function of an altitude, latitude, longitude, and solar modulation. We extracted electron spectra at an altitude  $h$  of 300–2000 m, and then integrated the spectra to obtain the electron fluxes  $F_{\text{seed}}$  in the energy range of 0.3–50.0 MeV. The electron flux was found to increase exponentially as a positive function of altitude, given by  $F_{\text{seed}} = 2.56 \times 10^{-3} \times \exp(h/1890 \text{ m})$  electrons  $\text{cm}^{-2} \text{ s}^{-1}$ .

Carlson et al.<sup>57</sup> have considered 1 MeV seed electrons produced by cosmic rays. Kelley et al.<sup>22</sup> employed it, and derived the seed flux to be  $0.25 \text{ cm}^{-2} \text{ s}^{-1}$  at

14.1 km. Our calculation with EXPACS gives the electron flux at 14.1 km of  $0.86 \text{ cm}^{-2} \text{ s}^{-1}$ . Given that Carlson et al. took a more thorough approach than ours by simulating the effective seeding efficiency for various particles, energies, and geometries, our method might have overestimated the seed electron flux. Regardless of the potential errors in our method, our conclusion that the gamma-ray glow requires relativistic feedback is unaffected, because overestimation of the seed flux, even if it was the case, would result in an underestimation of the multiplication factor.

### Data Availability

The data sets generated and analysed during the current study are available from the corresponding author on request.

Received: 23 January 2019 Accepted: 22 May 2019

Published online: 25 June 2019

### References

- McCarthy, M. & Parks, G. K. Further observations of x-rays inside thunderstorms. *Geophys. Res. Lett.* **12**, 393–396 (1985).
- Fishman, G. J. et al. Discovery of intense gamma-ray flashes of atmospheric origin. *Science* **264**, 1313–1316 (1994).
- Smith, D. M., Lopez, L. I., Lin, R. P. & Barrington-Leigh, C. P. Terrestrial gamma-ray flashes observed up to 20 mev. *Science* **307**, 1085–1088 (2005).
- Marisaldi, M. et al. Detection of terrestrial gamma ray flashes up to 40 mev by the agile satellite. *J. Geophys. Res. Space Phys.* **115**, <https://doi.org/10.1029/2009JA014502> (2010).
- Briggs, M. S. et al. First results on terrestrial gamma ray flashes from the fermi gamma-ray burst monitor. *J. Geophys. Res. Space Phys.* **115**, <https://doi.org/10.1029/2009JA015242> (2010).
- Briggs, M. S. et al. Electron-positron beams from terrestrial lightning observed with fermi gbm. *Geophys. Res. Lett.* **38**, <https://doi.org/10.1029/2010GL046259> (2011).
- Tavani, M. et al. Terrestrial gamma-ray flashes as powerful particle accelerators. *Phys. Rev. Lett.* **106**, <https://doi.org/10.1103/PhysRevLett.106.018501> (2011).
- Mailyan, B. G. et al. The spectroscopy of individual terrestrial gamma-ray flashes: constraining the source properties. *J. Geophys. Res. Space Phys.* **121**, 11346–11363 (2016).
- Dwyer, J. R. et al. A ground level gamma-ray burst observed in association with rocket-triggered lightning. *Geophys. Res. Lett.* **31**, <https://doi.org/10.1029/2003GL018771> (2004).
- Dwyer, J. R. et al. Observation of a gamma-ray flash at ground level in association with a cloud-to-ground lightning return stroke. *J. Geophys. Res. Space Phys.* **117**, <https://doi.org/10.1029/2012JA017810> (2012).
- Tran, M. et al. A terrestrial gamma-ray flash recorded at the lightning observatory in Gainesville, Florida. *J. Atmos. Sol. Terr. Phys.* **136**, 86–93 (2015).
- Hare, B. M. et al. Ground-level observation of a terrestrial gamma ray flash initiated by a triggered lightning. *J. Geophys. Res. Atmospheres* **121**, 6511–6533 (2016).
- Bowers, G. S. et al. Gamma ray signatures of neutrons from a terrestrial gamma ray flash. *Geophys. Res. Lett.* **44**, 10063–10070 (2017).
- Enoto, T. et al. Photonuclear reactions triggered by lightning discharge. *Nature* **551**, 481–484 (2017).
- Abbasi, R. et al. The bursts of high energy events observed by the telescope array surface detector. *Phys. Lett. A* **381**, 2565–2572 (2017).
- Abbasi, R. U. et al. Gamma ray showers observed at ground level in coincidence with downward lightning leaders. *J. Geophys. Res. Atmospheres* **123**, 6864–6879 (2018).
- Smith, D. M. et al. Characterizing upward lightning with and without a terrestrial gamma-ray flash. *J. Geophys. Res. Atmospheres*, <https://doi.org/10.1029/2018jd029105> (2018).
- Rutjes, C., Diniz, G., Ferreira, I. S. & Ebert, U. Tgf afterglows: a new radiation mechanism from thunderstorms. *Geophys. Res. Lett.* **44**, 10702–10712 (2017).
- Torii, T., Sugita, T., Kamogawa, M., Watanabe, Y. & Kusunoki, K. Migrating source of energetic radiation generated by thunderstorm activity. *Geophys. Res. Lett.* **38**, <https://doi.org/10.1029/2011GL049731> (2011).
- Chilingarian, A., Hovsepyan, G. & Hovhannissyan, A. Particle bursts from thunderclouds: natural particle accelerators above our heads. *Phys. Rev. D* **83**, <https://doi.org/10.1103/PhysRevD.83.062001> (2011).
- Eack, K. B., Beasley, W. H., Rust, W. D., Marshall, T. C. & Stolzenburg, M. Initial results from simultaneous observation of x-rays and electric fields in a thunderstorm. *J. Geophys. Res. Atmospheres* **101**, 29637–29640 (1996).
- Kelley, N. A. et al. Relativistic electron avalanches as a thunderstorm discharge competing with lightning. *Nat. Commun.* **6**, 7845 (2015).
- Kochkin, P. et al. In-flight observation of gamma ray glows by ildas. *J. Geophys. Res. Atmospheres*, <https://doi.org/10.1002/2017JD027405> (2017).
- Brunetti, M., Cecchini, S., Galli, M., Giovannini, G. & Pagliarin, A. Gamma-ray bursts of atmospheric origin in the mev energy range. *Geophys. Res. Lett.* **27**, 1599–1602 (2000).
- Torii, T. et al. Gradual increase of energetic radiation associated with thunderstorm activity at the top of Mt. Fuji. *Geophys. Res. Lett.* **36**, <https://doi.org/10.1029/2008GL037105> (2009).
- Tsuchiya, H. et al. Observation of an energetic radiation burst from mountain-top thunderclouds. *Phys. Rev. Lett.* **102**, <https://doi.org/10.1103/PhysRevLett.102.255003> (2009).
- Tsuchiya, H. et al. Observation of thundercloud-related gamma rays and neutrons in Tibet. *Phys. Rev. D* **85**, <https://doi.org/10.1103/PhysRevD.85.092006> (2012).
- Chilingarian, A. et al. Ground-based observations of thunderstorm-correlated fluxes of high-energy electrons, gamma rays, and neutrons. *Phys. Rev. D* **82**, <https://doi.org/10.1103/PhysRevD.82.043009> (2010).
- Chilingarian, A., Hovsepyan, G. & Mnatsakanyan, E. Mount Aragats as a stable electron accelerator for atmospheric high-energy physics research. *Phys. Rev. D* **9**, <https://doi.org/10.1103/PhysRevD.93.052006> (2016).
- Torii, T., Takeishi, M. & Hosono, T. Observation of gamma-ray dose increase associated with winter thunderstorm and lightning activity. *J. Geophys. Res. Atmospheres* **107**, ACL 2-1–ACL 2-13 (2002).
- Tsuchiya, H. et al. Detection of high-energy gamma rays from winter thunderclouds. *Phys. Rev. Lett.* **99**, <https://doi.org/10.1103/PhysRevLett.99.165002> (2007).
- Tsuchiya, H. et al. Long-duration  $\text{F}^{\pm}$  ray emissions from 2007 and 2008 winter thunderstorms. *J. Geophys. Res.* **116**, <https://doi.org/10.1029/2010JD015161> (2011).
- Kuroda, Y. et al. Observation of gamma ray bursts at ground level under the thunderclouds. *Phys. Lett. B* **758**, 286–291 (2016).
- Alexeenko, V., Khaerdinov, N., Lidvansky, A. & Petkov, V. Transient variations of secondary cosmic rays due to atmospheric electric field and evidence for pre-lightning particle acceleration. *Phys. Lett. A* **301**, 299–306 (2002).
- Tsuchiya, H. et al. Hardening and termination of long-duration  $\text{F}^{\pm}$  rays detected prior to lightning. *Phys. Rev. Lett.* **111**, <https://doi.org/10.1103/PhysRevLett.111.015001> (2013).
- Chilingarian, A., Hovsepyan, G., Khanikyan, G., Reymers, A. & Soghomonian, S. Lightning origination and thunderstorm ground enhancements terminated by the lightning flash. *Europhys. Lett.* **110**, 49001 (2015).
- Chilingarian, A. et al. Types of lightning discharges that abruptly terminate enhanced fluxes of energetic radiation and particles observed at ground level. *J. Geophys. Res. Atmospheres* **122**, 7582–7599 (2017).
- Wada, Y. et al. Termination of electron acceleration in thundercloud by intracloud/intercloud discharge. *Geophys. Res. Lett.* **45**, 5700–5707 (2018).
- Gurevich, A., Milikh, G. & Roussel-Dupre, R. Runaway electron mechanism of air breakdown and preconditioning during a thunderstorm. *Phys. Lett. A* **165**, 463–468 (1992).
- Dwyer, J. R. A fundamental limit on electric fields in air. *Geophys. Res. Lett.* **30**, <https://doi.org/10.1029/2003GL017781> (2003).
- Wilson, C. T. R. The acceleration of  $\text{F}^{\pm}$ -particles in strong electric fields such as those of thunderclouds. *Math. Proc. Camb. Philos. Soc.* **22**, 534 (1925).
- Dwyer, J. R. The relativistic feedback discharge model of terrestrial gamma ray flashes. *J. Geophys. Res. Space Phys.* **117**, <https://doi.org/10.1029/2011JA017160> (2012).
- Umamoto, D. et al. On-ground detection of an electron-positron annihilation line from thunderclouds. *Phys. Rev. E* **93**, <https://doi.org/10.1103/PhysRevE.93.021201> (2016).
- Enoto, T. et al. Multi-point measurement campaigns of gamma rays from thunderclouds and lightning in Japan. In *Proc. XVI International Conference on Atmospheric Electricity* (2018).
- Goto, Y. & Narita, K. Observations of winter lightning to an isolate tower. *Res. Lett. Atmos. Electr.* **12**, 57–60 (1992).
- Rakov, V. A. & Uman, M. A. *Lightning: Physics and Effects* (Cambridge University Press, Cambridge, 2003).
- Agostinelli, S. et al. Geant4—a simulation toolkit. *Nucl. Instrum. Methods Phys. Res. A* **506**, 250–303 (2003).
- Arnaud, K. A. XSPEC: the first ten years. In *Astronomical Data Analysis Software and Systems V*, vol. 101 of *Astronomical Society of the Pacific Conference Series* (eds. Jacoby, G. H. & Barnes, J.), 17 (1996). <http://adsabs.harvard.edu/abs/1996ASPC...101...17A>.
- Dwyer, J. R. & Babich, L. P. Low-energy electron production by relativistic runaway electron avalanches in air. *J. Geophys. Res. Space Physics* **116**, <https://doi.org/10.1029/2011JA016494> (2011).
- Dwyer, J. R. Relativistic breakdown in planetary atmospheres. *Phys. Plasmas* **14**, 042901 (2007).

51. Babich, L. P. Generation of neutrons in giant upward atmospheric discharges. *JETP Lett.* **84**, 285–288 (2006).
52. Babich, L. P. Neutron generation mechanism correlated with lightning discharges. *Geomagn. Aeron.* **47**, 664–670 (2007).
53. Carlson, B. E., Lehtinen, N. G. & Inan, U. S. Neutron production in terrestrial gamma ray flashes. *J. Geophys. Res. Space Phys.* **115**, <https://doi.org/10.1029/2009JA014696> (2010).
54. Dwyer, J. R., Smith, D. M. & Cummer, S. A. High-energy atmospheric physics: terrestrial gamma-ray flashes and related phenomena. *Space Sci. Rev.* **173**, 133–196 (2012).
55. Sato, T. Analytical model for estimating terrestrial cosmic ray fluxes nearly anytime and anywhere in the world: extension of parma/expacs. *PLoS ONE* **10**, e0144679 (2015).
56. Sato, T. Analytical model for estimating the zenith angle dependence of terrestrial cosmic ray fluxes. *PLoS ONE* **11**, e0160390 (2016).
57. Carlson, B. E., Lehtinen, N. G. & Inan, U. S. Runaway relativistic electron avalanche seeding in the earth's atmosphere. *J. Geophys. Res. Space Phys.* **113**, <https://doi.org/10.1029/2008JA013210> (2008).

## Acknowledgements

We thank K. Watarai, K. Yoneguchi, K. Kimura, K. Kitano, and K. Kono for detector deployment; H. Sakurai, M. Niikura, and the Sakurai group members at RIKEN Nishina Center for providing Bi<sub>4</sub>Ge<sub>3</sub>O<sub>12</sub> scintillation crystals; T. Nagao, T. Suzuki, and H. Fujiwara for providing lightning and weather data; T. Nakano, T. Tamagawa, A. Bamba, H. Odaka, and P. Laurent for project supports and discussions; and S. Otsuka and H. Kato for supporting detector developments. Deployment of LF stations is supported by Uozu City, Himi City, and Nyuzen Town in Toyama Prefecture. The ELF observation system at Kujū is maintained by International Center for Space Weather Science and Education (ICSWSE) in Kyushu University. This research is supported by JSPS/MEXT KAKENHI grants 15K05115, 15H03653, 16H04055, 16H06006, 16K05555, 17K05659, 18J13355, 18H01236, 19H00683, by Hakubi project and SPIRITS 2017 of Kyoto University, and by the joint research program of the Institute for Cosmic Ray Research (ICRR), the University of Tokyo. The startup phase of the multi-point observation project is supported via an academic crowdfunding platform “academist” by Y. Shikano, Y. Araki, M. T. Hayashi, N. Matsumoto, T. Enoto, K. Hayashi, S. Koga, T. Hamaji, Y. Torisawa, S. Sawamura, J. Purser, S. Suehiro, S. Nakane, M. Konishi, H. Takami, T. Sawara, and all of the supporters. The crowdfunding activity is supported by “adachi design laboratory”. The Monte Carlo simulations were performed on HOKUSAI GreatWave and BigWaterfall supercomputing systems operated by RIKEN Advanced Center for Computing and Communication. The background images in Fig. 1 and Supplementary Fig. 3a were provided by the Geospatial Information Authority of Japan. The XRAIN data obtained by Japan Ministry of Land, Infrastructure,

Transport and Tourism was retrieved from Data Integration and Analysis System (DIAS) operated by the University of Tokyo.

## Author contributions

Y.W., T.E., Y.F., T.Y., K.N., T. Matsumoto, and H.T. were responsible for the radiation detector developments, data analysis, and interpretation; T.E. is the project leader of the multi-point observation; Y.W. led the detector development, installation, analysis, simulations, and prepared the draft of the manuscript; Y.F. verified the Monte Carlo simulations using Geant4; T.Y. led the development of the data acquisition system; Y.N. and T. Morimoto were responsible for the LF observation; M.S. was responsible for the ELF observation; D.Y. and T.S. contributed to the radiation detector operation; H.S. contributed to operation of the LF stations; K.N., M.K., T.U., K.M., and H.T. contributed to the data interpretation.

## Additional information

**Supplementary information** accompanies this paper at <https://doi.org/10.1038/s42005-019-0168-y>.

**Competing interests:** The authors declare no competing interests.

**Reprints and permission** information is available online at <http://npg.nature.com/reprintsandpermissions/>

**Publisher's note:** Springer Nature remains neutral with regard to jurisdictional claims in published maps and institutional affiliations.



**Open Access** This article is licensed under a Creative Commons Attribution 4.0 International License, which permits use, sharing, adaptation, distribution and reproduction in any medium or format, as long as you give appropriate credit to the original author(s) and the source, provide a link to the Creative Commons license, and indicate if changes were made. The images or other third party material in this article are included in the article's Creative Commons license, unless indicated otherwise in a credit line to the material. If material is not included in the article's Creative Commons license and your intended use is not permitted by statutory regulation or exceeds the permitted use, you will need to obtain permission directly from the copyright holder. To view a copy of this license, visit <http://creativecommons.org/licenses/by/4.0/>.

© The Author(s) 2019